

Near-Earth object intercept trajectory design for planetary defense



George Vardaxis^{a,*}, Bong Wie^{b,1}

^a Iowa State University, 2348 Howe Hall, Ames, IA 50011-2271, USA

^b Iowa State University, 2271 Howe Hall, Ames, IA 50011-2271, USA

ARTICLE INFO

Article history:

Received 30 August 2013

Received in revised form

3 March 2014

Accepted 6 April 2014

Available online 13 April 2014

Keywords:

Mission design

Planetary defense

Gravitational simulator

Encounter geometry

Keyholes

ABSTRACT

Tracking the orbit of asteroids and planning for asteroid missions have ceased to be a simple exercise, and become more of a necessity, as the number of identified potentially hazardous near-Earth asteroids increases. Several software tools such as Mystic, MALTO, Copernicus, SNAP, OTIS, and GMAT have been developed by NASA for spacecraft trajectory optimization and mission design. However, this paper further expands upon the development and validation of an Asteroid Mission Design Software Tool (AMiDST), through the use of approach and post-encounter orbital variations and analytic keyhole theory. Combining these new capabilities with that of a high-precision orbit propagator, this paper describes fictional mission trajectory design examples of using AMiDST as applied to a fictitious asteroid 2013 PDC-E. During the 2013 IAA Planetary Defense Conference, the asteroid 2013 PDC-E was used for an exercise where participants simulated the decision-making process for developing deflection and civil defense responses to a hypothetical asteroid threat.

© 2014 IAA. Published by Elsevier Ltd. All rights reserved.

1. Introduction

Traditional trajectory and mission optimization tools (such as Mystic, MALTO, Copernicus, SNAP, OTIS, and GMAT) are high-fidelity computer programs being developed by NASA [1,2]. A commonality of all these tools is that they primarily look at the intermediate stage of a mission, the mission trajectory from the current location to desired target – more or less overlooking the other two stages of any mission design, in comparison. An on-line mission design tool to aid in the design and understanding of kinetic impactors necessary for guarding against objects on an Earth-impacting trajectory is being developed at The

Aerospace Corporation [3]. Still under development, this on-line tool has hopes of incorporating several specific design variables and limitations to allow for only feasible mission designs based on current launch and mission capabilities.

The Asteroid Mission Design Software Tool (AMiDST) being developed at the Asteroid Deflection Research Center (ADRC) at Iowa State University [4–6] does not yet have the high fidelity as many existing optimization-based packages. However, the focus of the program lies on the launch and terminal phase of a near-Earth object (NEO) mission rather than finding the optimal mission trajectory. Looking into several launch vehicle and spacecraft configurations to complete a given mission design to a designated target NEO, the AMiDST evaluates the possible combinations based upon several evaluation criteria such as launch vehicle mass capacity, mission ΔV requirements, and excess launch vehicle ΔV . In addition to these features, it also provides the estimated total mission cost, used as a main determining factor between mission configurations.

* Corresponding author.

E-mail addresses: vardaxis@iastate.edu (G. Vardaxis), bongwie@iastate.edu (B. Wie).

¹ Asteroid Deflection Research Center, Department of Aerospace Engineering.

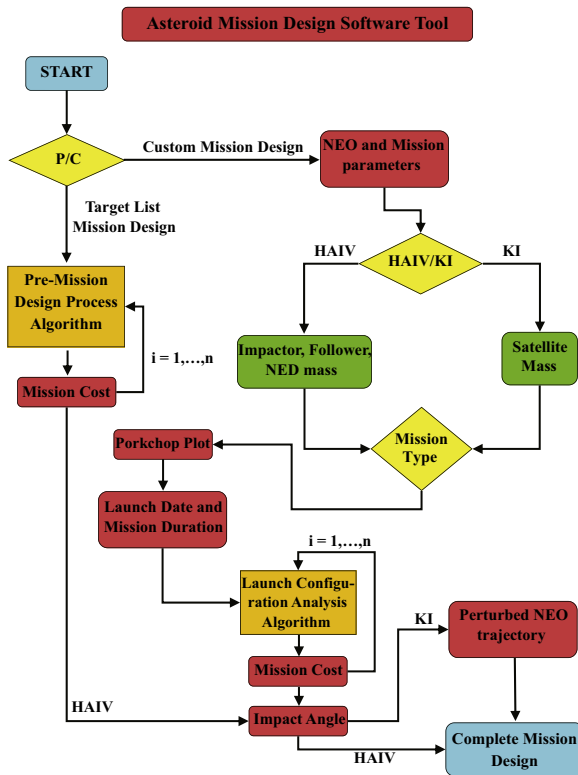


Fig. 1. Flowchart illustration of the AMiDST.

A flowchart illustration of the basic algorithms used by AMiDST is presented in Fig. 1. In this figure, HAIV stands for Hypervelocity Asteroid Intercept Vehicle and KI for Kinetic Impactor, and NED for Nuclear Explosive Device, described in detail by Pitz et al. [7,8].

For a current version of AMiDST, the terminal phase of a NEO mission is limited, at this time, to kinetic impact perturbations applied to the target NEO's orbital trajectory. Taking the output of the mission analysis of relative impact angle and velocities of both the spacecraft and target NEO, along with the mass of both objects, the trajectory of the perturbed asteroid would be tracked in order to find how much the trajectory is altered from the previous unperturbed orbit. In addition to simply tracking the NEO to a future time, a resonance and keyhole analysis would be performed to see the likelihood the body would have a further future threat to the Earth.

2. Intercept trajectory design for asteroids with no keyholes

Near-Earth objects are asteroids and comets with perihelion distance (q) less than 1.3 astronomical units (AU). The vast majority of NEOs are asteroids, which are referred to as near-Earth asteroids (NEAs). NEAs are divided into three groups (Aten, Apollo, Amor) based on their perihelion distance, aphelion distance (Q), and semi-major axes (a). Of these three classes of asteroids, Aten and Apollo type asteroids are of particular interest to this study due to their relative proximity and Earth impacting potential. Atens are Earth-crossing NEAs

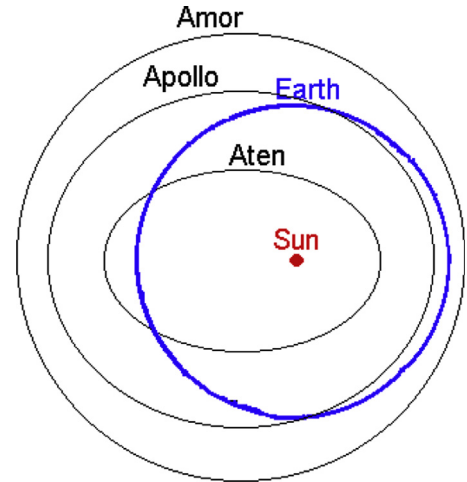


Fig. 2. Typical orbits of Apollo, Aten, and Amor asteroids.

with semi-major axes smaller than Earth's ($a < 1.0$ AU, $Q > 0.983$ AU). Apollos are Earth-crossing NEAs with semi-major axes larger than Earth's ($a > 1.0$ AU, $q < 1.017$ AU) [9]. Fig. 2 shows representative orbits for the three class of asteroids in reference to Earth's orbit. With the wide array of choices to select target NEOs from, there have been many objects studied through the use of AMiDST [4–6]. The most notable targets being Apophis, 1999 RQ36, 2011 AG5, 2012 DA14, and comet 2013 A1.

In 1990, Congress directed NASA to increase the rate of discovery of near Earth objects [10]. Through those efforts, at times objects of significant size have been found to be on a potential Earth-impacting trajectory. The accurate prediction of such Earth-impacting trajectories could be obtained through the use of high-fidelity N-body models, also containing the effects of non-gravitational orbital perturbations such as solar radiation pressure (SRP). From such highly precise asteroid orbits, many advantages can be had: more specific mission planning, higher certainty of the target's location, and more accurate impact probability.

2.1. Orbit simulation

The orbital motion of an asteroid is governed by a so-called Standard Dynamical Model (SDM) of the form

$$\frac{d^2 \mathbf{r}}{dt^2} = -\frac{\mu}{r^3} \mathbf{r} + \sum_{k=1}^n \mu_k \left(\frac{\mathbf{r}_k - \mathbf{r}}{|\mathbf{r}_k - \mathbf{r}|^3} - \frac{\mathbf{r}_k}{r_k^3} \right) + \mathbf{f} \quad (1)$$

where $\mu = GM$ is the gravitational parameter of the Sun, n is the number of perturbing bodies, μ_k and \mathbf{r}_k are the gravitational parameter and heliocentric position vector of perturbing body k , respectively, and \mathbf{f} represents other non-conservative orbital perturbation acceleration. The gravitational model used in orbit propagation takes into account the effects of the Sun, all eight planets, Earth's Moon, Pluto, Ceres, Pallas, and Vesta.

Previous studies performed at the ADRC were concerned with the impact probability of potential Earth-impacting asteroids, such as Apophis, 1999 RQ36, and 2011 AG5 due to their proximity to Earth and their relatively high impact

probability. Using commercial software such as NASA's General Mission Analysis Tool (GMAT), AGI's Satellite Tool Kit (STK), and Jim Baer's Comet/asteroid Orbit Determination and Ephemeris Software (CODES), the ADRC conducted precision orbital simulation studies to compare with JPL's Sentry program [11].

2.2. Previous work

Taking Apophis as a reference NEO, simulations have been run from an initial epoch of August 27, 2011 until January 1, 2037 to show the capabilities of the ADRC's N-body code in calculating precise, long-term orbit trajectories. A preliminary test was conducted for the period of May 23, 2029 to May 13, 2036 that show the relative errors of GMAT and STK to JPL's Sentry (Horizons), as well as the error of the N-body code with respect to Sentry. The error in the radial position of Apophis between the N-body code to that of JPL's Sentry is much lower than that of both GMAT and STK. The N-body simulator used to obtain the aforementioned results uses a Runge–Kutta Fehlberg (RKF) 7(8) fixed-timestep method, including the orbital perturbations of all eight planets, Pluto, and Earth's Moon, in the form of constant orbital element rates coupled with the nominal element values provided updated position and velocity data for the perturbation bodies [4].

2.3. Current work and capabilities

The fixed timestep numerical integration algorithm has been changed to a variable step method, expanding upon the work done on the numerical integration scheme used to obtain the results previously discussed. The Runge–Kutta Fehlberg method is used for approximating the solution of a differential equation $\dot{x}(t) = f(x, t)$ with initial condition $x(t_0)$. The implementation evaluates $f(x, t)$ 13 times per step using embedded seventh-order and eighth-order Runge–Kutta estimates to estimate not only the solution but also the error. By specifying the interval in which the results of the integration should be reported and the acceptable local error tolerance, the algorithm takes as many error controlled steps as necessary to calculate the state vector at the desired time.

Orbital data from all chosen planetary bodies, in the International Celestial Reference Frame (ICRF) 2000 with the Sun's center set as the origin of the coordinate frame, is taken for a given period of time to construct a planetary state vector (X, Y, Z, V_X, V_Y, V_Z) database using ephemeris data from the NASA Jet Propulsion Laboratory (JPL) Horizons website. An interpolation scheme is constructed in order to accommodate the need to retrieve data at any specified date within the propagation time period. Using the Julian Date of the available state vector data for each planet as the distinct independent variables of an n -th degree interpolating polynomial, a unique polynomial $P(x)$ is created for each state, which is then applied to each body.

The three most well-known non-conservative perturbations are solar radiation pressure (SRP), relativistic effects, and the Yarkovsky effect – the former two being the most prevalent. Solar radiation pressure provides a radial outward force on the asteroid body from the interaction of the

Sun's photons impacting the asteroid surface. A SRP model is given by

$$\mathbf{a}_{SRP} = (K)(C_R) \left(\frac{A_R}{M} \right) \left(\frac{L_S}{4\pi c r^3} \right) \mathbf{r} \quad (2)$$

where \mathbf{a}_{SRP} is the acceleration vector due to the solar radiation pressure, C_R is the coefficient for solar radiation, A_R is the cross-sectional area presented to the Sun, M is the mass of the asteroid, K is the fraction of the solar disk visible at the asteroid's location, L_S is the luminosity of the Sun, c is the speed of light, and \mathbf{r} and r is the distance vector and magnitude of the asteroid from the Sun, respectively.

The relativistic effects of the body are included because for many objects, especially those with small semi-major axes and large eccentricities, those effects introduce a non-negligible radial acceleration toward the Sun. One form of the relativistic effects is represented by

$$\mathbf{a}_R = \frac{k^2}{c^2 r^3} \left[\frac{4k^2 \mathbf{r}}{r} - (\dot{\mathbf{r}} \cdot \dot{\mathbf{r}}) \mathbf{r} + 4(\mathbf{r} \cdot \dot{\mathbf{r}}) \dot{\mathbf{r}} \right] \quad (3)$$

where \mathbf{a}_R is the acceleration vector due to relativistic effects, k is the Gaussian constant, \mathbf{r} is the position vector of the asteroid, and $\dot{\mathbf{r}}$ is the velocity vector of the asteroid.

With the introduction of such non-conservative forces the error within the system will increase, but these effects need to be included in calculations in order to maintain consistency with the planetary ephemeris. A more complete dynamical model will allow the accurate calculation of asteroid impact probabilities and gravitational keyholes, leading to more effective mission designs [12].

2.4. AMiDST features

Some of the main features of AMiDST's trajectory design capabilities are highlighted here.

2.4.1. Pre-determined target list

The pre-determined target list option within the program is meant more as an introduction to some of AMiDST's capabilities. A launch date is given for each individual asteroid, leaving no need for too much user input. With the launch date determined and the target defined then the spacecraft's orbital trajectory is well-defined and no longer a concern. The AMiDST analyzes all the possible launch configurations available to complete the mission, the arrival at the target NEO, and the estimated mission costs. The outputs are then made available for the user to examine and understand the results of the NEO mission design analyses. Original mission designs focused on three class of mission payloads (300-kg NED, 1000-kg NED, and 1500-kg NED) within the HAIV spacecraft concept. The results listed in this section of the program are not limited to a single design between these three mission payloads, but include all three, and highlight the best mission configuration for each type.

2.4.2. Custom mission trajectory design

For custom mission designs, the user begins by entering information about the target NEO of interest and the low-Earth orbit (LEO) departure radius. Then the choice is given between two types of spacecraft to be used for the

mission, the HAIV concept or a Kinetic Impactor (KI). For the HAIV spacecraft, information about the mass of the impactor, follower, and NED are obtained from the user, while in the KI spacecraft case the total mass of the satellite is needed. In either case, the user is prompted with a decision between three mission types: a direct intercept at a relative speed of 10 km/s, or rendezvous. The software tool then loads the appropriate porkchop plot, showing the total required mission ΔV , where the user can select as many design points as desired, resulting in a set of launch dates and mission durations. Given the launch date(s) and mission duration(s), the transfer orbit between Earth and the target NEO is completely determined by Lambert's Problem, allowing the possible launch configurations for the mission(s) to be analyzed along with their estimated mission cost and compared to come up with the preferred launch configuration for each given mission. The resulting mission trajectories for either the HAIV or the KI spacecraft are provided along with the arrival impact angles. Since the purpose of the HAIV design was total NEO disruption, the trajectory of the remaining asteroid fragments are not tracked (although such an analysis can be conducted), however in the case of the KI spacecraft the slightly perturbed NEO is propagated forward in time to see how much the orbit has changed from the original, before the impulse was applied.

2.4.3. Mission cost estimate

Mission cost estimation to design and fabricate the missions is an important task necessary for an early assessment of the mission viability and feasibility. A staple of this mission design tool is the evaluation of estimated total mission cost, the determining factor between mission configurations in the cases where more than one launch configuration can result in a successful mission. A cost estimation algorithm was developed to determine the costs associated with constructing the HNIS, based on a number of previous spacecraft missions with similar goals and parameters. Spacecraft such as Deep Impact, Stardust, and Dawn were researched to find the cost of developing their spacecraft and a linear polynomial fit was applied to the data to come up with an analytic formula relating spacecraft mass and cost. Before the results of the cost estimation algorithm are discussed, it is important to note that the mass/cost of the NED was not included when the estimations were made. In addition, the total mass margin was left intact when estimating the cost of the HAIV development, in order for the estimate to be thought of as a relative maximum.

A similar analysis was also run using NASA's Advanced Mission Cost Model (AMCM) [13], to get a rough-order-of-magnitude approximation for the costs of these three missions. The estimates from the AMCM are really rough though, mostly due to the fact that these HAIV designs do not exactly fit into a single mission category from the available choices. However, the estimates from AMCM at least verify that the estimates from AMiDST are in the appropriate cost range. More detailed discussions on cost estimates as well as technical assessments of a variety of NEO deflection/disruption missions can be found in Refs. [13] and [14].

3. Keyholes for planetary defense mission design

When a body undergoes an encounter with a planet, there are a number of ways that its orbit will be affected. The environment around a planet is very dynamic in nature, and small inaccuracies in modeling can result in drastic differences between the simulated trajectories and the actual trajectory. Getting a good understanding behind the geometry of planetary close-approaches and the effect that they have on the orbital elements of the bodies that undergo them should assist with the task of predicting the resulting orbital trajectory after a close flyby of a planet. In some cases, upon having a close approach with a planet the asteroid will pass through what is called a gravitational keyhole. As will be discussed later in this paper, asteroid 2013 PDC-E ends up having a close-encounter with the Earth and travels through a keyhole in its encounter target plane. A brief description of analytic keyhole theory and target planes is provided in the Appendix, but for now we will discuss the variation in orbital elements due to planetary close-encounters.

3.1. Basic assumptions

The dynamical system under consideration in the following analysis consists of the Sun, a planet orbiting the Sun on a circular orbit, and an asteroid, viewed as a particle, that is on an eccentric and inclined orbit around the Sun that crosses the orbit of the planet. Assume the planet has an orbital radius $R=1$, the product $k\sqrt{M}=1$, where k is the Gaussian constant and M is the mass of the Sun, and the asteroid has orbital parameters $(a, e, i, \omega, \Omega)$. In order to have the asteroid cross the orbital path of the planet, the asteroid must meet the following criteria: $a(1-e) < 1 < a(1+e)$. The frame of reference established for this analysis is centered on the planet, the x -axis points radially opposite to the Sun, the y -axis is the direction of motion of the planet itself, and the z -axis completes the right-handed system by pointing in the direction of the planet's angular momentum vector – illustrated in Fig. 3. The three most important orbital elements used in the analysis are the semi-major axis a , the eccentricity e , and the inclination i .

3.2. Relationship between orbital parameters a, e, i and U, ϕ, θ

Let $\mathbf{U} = (U_x, U_y, U_z)$ and U be the relative velocity vector and the magnitude between the planet and the asteroid [15], defined as

$$U = \sqrt{3 - \left[\frac{1}{a} + 2\sqrt{a(1-e^2)} \cos i \right]} \quad (4)$$

$$U_x = U \sin \theta \sin \phi \quad (5)$$

$$U_y = U \cos \theta \quad (6)$$

$$U_z = U \sin \theta \cos \phi \quad (7)$$

where θ and ϕ are the angles that define the direction of U by

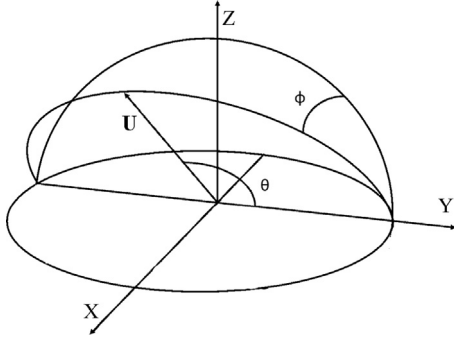


Fig. 3. Reference frame of \mathbf{U} . The origin is placed at the planet's center, the positive x -axis is opposite the direction of the Sun, the y -axis is in the direction of the planet's motion, and the z -axis is parallel to the planet's angular momentum vector. The angles ϕ and θ define the direction of \mathbf{U} .

$$\phi = \tan^{-1} \left[\pm \sqrt{\frac{2a-1}{a^2(1-e^2)}} - 1 \frac{1}{\sin i} \right] \quad (8)$$

$$\theta = \cos^{-1} \left[\frac{1-U^2-1/a}{2U} \right] \quad (9)$$

where θ may vary between 0 and π , and ϕ between $-\pi/2$ and $\pi/2$.

In terms of a , e , and i , the components of \mathbf{U} are given by

$$U_x = \left[2 - \frac{1}{a} - a(1-e^2) \right]^{1/2} \quad (10)$$

$$U_y = \sqrt{a(1-e^2)} \cos i - 1 \quad (11)$$

$$U_z = \sqrt{a(1-e^2)} \sin i \quad (12)$$

and, inversely, we have

$$a = \frac{1}{1-U^2-2U_y} \quad (13)$$

$$e = [U^4 + 4U_y^2 + U_x^2(1-U^2-2U_y) + 4U^2U_y]^{1/2} \quad (14)$$

$$i = \sin^{-1} \sqrt{U_z^2/[U_z^2 + (1+U_y)^2]} \quad (15)$$

Within the scope of potential impacting bodies, one of the most important regions of the planetocentric system defined by the body's orbital elements is the B-plane (discussed in detail in [Appendix A](#)). Looking back at [Fig. 3](#), it can be seen that the angles ϕ and θ are defined within the planetocentric reference frame (X , Y , Z) with respect to the relative velocity vector \mathbf{U} . So, if a reference frame (ξ , η , ζ) is defined on the B-plane of the encounter, then the angles θ and ϕ can be used to transform between the two reference frames. This coordinate transformation is accomplished by first rotating through an angle $-\phi$ about Y and then rotating through an angle $-\theta$ about ξ (perpendicular to the old Y -axis and to \mathbf{U}). In matrix notation, the coordinate transformation can be written as

$$\begin{bmatrix} \xi \\ \eta \\ \zeta \end{bmatrix} = \mathbf{R}_\xi(-\theta) \mathbf{R}_Y(-\phi) \begin{bmatrix} X \\ Y \\ Z \end{bmatrix} \quad (16)$$

and the inverse transformation can be accomplished by rotating through the positive angles in reverse order [\[15\]](#).

3.3. Post-keyhole geometry

After the asteroid has an encounter with the target planet, the \mathbf{U} vector is rotated by an angle γ in the direction ψ , where ψ is the angle measured counter-clockwise from the meridian containing the \mathbf{U} vector, as seen in [Fig. 4](#). The deflection angle γ is related to the encounter parameter b by

$$\tan \frac{1}{2}\gamma = \frac{m}{bU^2} \quad (17)$$

where m is the mass of the planet, in units of the Sun's mass. The angle θ after the encounter, denoted by θ' , is calculated from

$$\cos \theta' = \cos \theta \cos \gamma + \sin \theta \sin \gamma \cos \psi \quad (18)$$

and, defining $\chi = \phi - \phi'$, we have

$$\sin \chi = \sin \psi \sin \gamma / \sin \theta' \quad (19)$$

$$\cos \chi = (\cos \gamma \sin \theta - \sin \gamma \cos \theta \cos \psi) / \sin \theta' \quad (20)$$

$$\tan \chi = \sin \psi \sin \gamma / (\cos \gamma \sin \theta - \sin \gamma \cos \theta \cos \psi) \quad (21)$$

$$\tan \phi' = (\tan \phi - \tan \chi) / (1 + \tan \phi \tan \chi) \quad (22)$$

Evaluating for the post-encounter variables θ' and ϕ' , the values of a' , e' , and i' can be obtained accordingly [\[15\]](#).

3.4. Post-keyhole orbital elements

In the case of asteroid 2013 PDC-E, the post-encounter orbital elements were given in addition to the pre-encounter elements, so an analysis of the post-encounter geometry is not needed. However, the scenario lends itself well as a learning exercise to show how the approach and post-encounter geometries relate to each other in the context of an Earth-threatening asteroid. The important orbital parameters to the analysis are given in [Table 1](#).

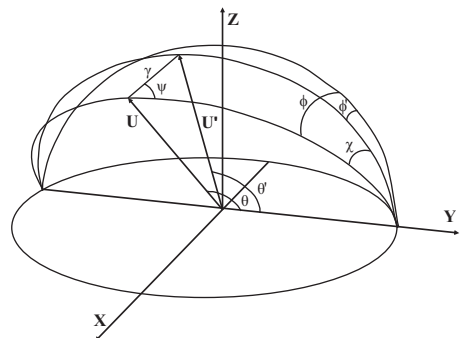


Fig. 4. Reference frame of \mathbf{U} and \mathbf{U}' . After the body's encounter with the planet, the vector \mathbf{U} is rotated by an angle γ in the direction of ψ .

3.4.1. Post-keyhole semi-major axis

Given that $|\mathbf{U}|$ is constant, the variation in the semi-major axis Δa depends only on the parameters θ and θ' as

$$\Delta a = \frac{a' - a}{a} = \frac{1 - U^2 - 2U \cos \theta}{1 - U^2 - 2U \cos \theta'} - 1 \quad (23)$$

Fig. 5 shows the variation in the semi-major axis a . The colors on the mesh depict the value of the variation, and the black dotted line depicts the resulting semi-major axis variation of 2013 PDC-E from its Earth encounter. From the figure, it can be seen that the asteroid is susceptible to having its semi-major axis increased or decreased, depending on the values of γ and ψ . Preliminary observations show that values of ψ between about $\pi/2$ and $3\pi/2$ will cause 2013 PDC-E to have a smaller post-encounter semi-major axis than its pre-encounter value. In this particular case, the change in semi-major axis is about 0.18 meaning that the value of ψ will come about to be smaller than $\pi/2$ or greater than $3\pi/2$.

3.4.2. Post-keyhole inclination

The tangent of inclination is defined as

$$\tan i = \frac{\cos \phi \sin \theta}{1/U + \cos \theta} = \frac{U_z}{1 + U_y} \quad (24)$$

and after the rotation of the relative velocity vector by the deflection angle γ in the direction of ψ , it becomes

$$\tan i' = \frac{\cos \phi \sin \theta \cos \gamma - \cos \phi \cos \theta \sin \gamma \cos \psi + \sin \phi \sin \gamma \sin \psi}{1/U + \cos \theta \cos \gamma + \sin \theta \sin \gamma \cos \psi} \quad (25)$$

The variation in inclination can be described by $\Delta i = \tan i' - \tan i$ [15]. Fig. 6 depicts the variation of the inclination of the

orbits of asteroid 2013 PDC-E. The black dotted line on the meshed grid shows the resulting variation of the inclination after the encounter with the Earth. The plot of post-encounter inclination variation has two distinct sections to it. When ψ is less than π the post-encounter inclination would be greater than the pre-encounter inclination, and when ψ is greater than π the inclination would decrease. The largest change in inclination seems to occur at ψ values of $\pi/2$ and $3\pi/2$.

3.4.3. Post-keyhole eccentricity

Recalling that

$$e^2 = U^4 + 4U_y^2 + U_x^2(1 - U^2 - 2U_y) + 4U^2U_y \quad (26)$$

the expression for the pre-encounter eccentricity of the asteroid orbit can be expressed in terms of the relative velocity magnitude and its components. Making a substitution for the corresponding post-encounter terms, the value of the eccentricity after the encounter with the target planet can be calculated as

$$e' = \sqrt{U'^4 + 4U_y'^2 + U_x'^2(1 - U'^2 - 2U_y') + 4U'^2U_y'} \quad (27)$$

Taking the difference between the post- and pre-encounter eccentricities shows the variation in the orbital eccentricity ($\Delta e = e' - e$) based on the planetary encounter. Fig. 7 depicts the variation of the eccentricity of asteroid 2013 PDC-E. The black dotted lines shown in the figure indicate the level of variation between the pre- and post-encounter eccentricities of the asteroid. The plot of eccentricity variation has a bit more complicated structure for this asteroid than the semi-major axis or inclination. Asteroid 2013 PDC-E would have more eccentric post-encounter orbits for values of ψ that approach the ends of the feasible domain $[0, 2\pi]$ and values near π . Values of ψ near $\pi/2$ and $3\pi/2$ seem to have a negative effect on the orbital eccentricities of the body. A closer look at the variation equations of (Δa , Δi , Δe) reveals cases where these equations can be further simplified, or interesting results become more apparent. Such an analysis is omitted in this paper. As is, this analysis only enables us to understand the potential variations in the orbital elements of a body having an encounter with the planet, to get a firm

Table 1

Orbital elements of asteroid 2013 PDC-E for pre-keyhole and post-keyhole.

Orbital element	Pre-keyhole	Post-keyhole
a	0.9846	1.1616
e	0.18831	0.22537
i	1.3941°	1.5311°

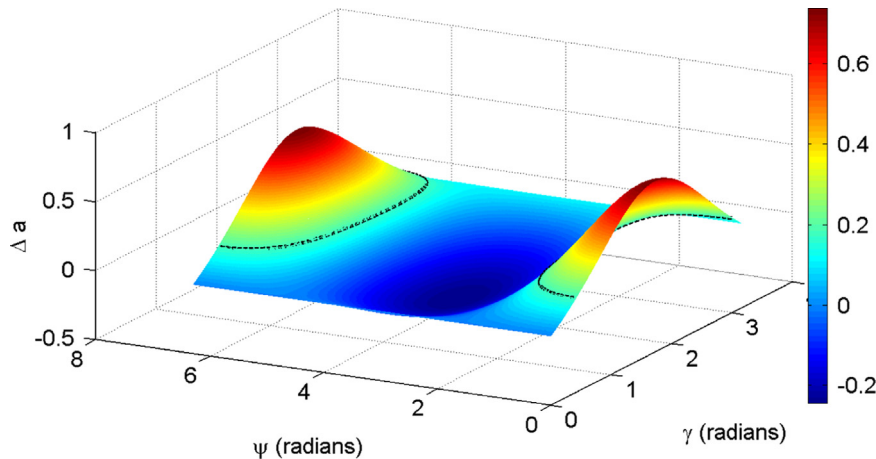


Fig. 5. Surface plot of variation of semi-major axis for asteroid 2013 PDC-E.

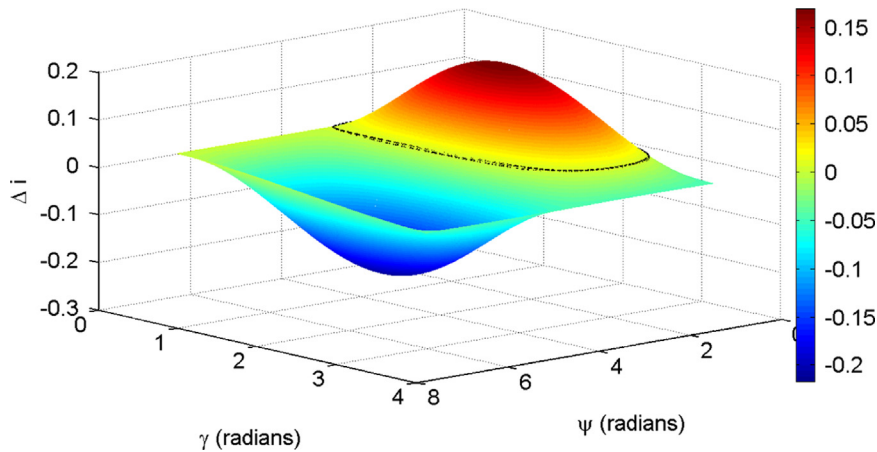


Fig. 6. Surface plot of variation of inclination for asteroid 2013 PDC-E.

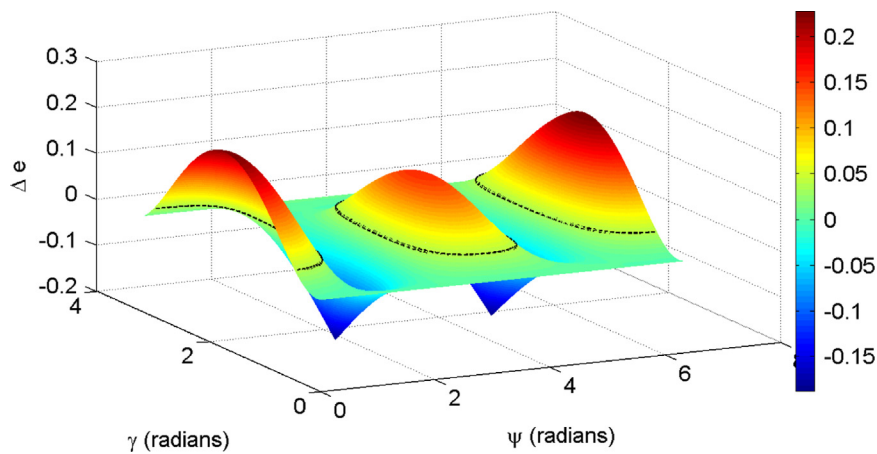


Fig. 7. Surface plot of variation of eccentricity for asteroid 2013 PDC-E.

grasp of the exact variation in the orbital elements would require either an analytic analysis of the encounter or a numerical approach to find the ψ and γ values.

4. Fictional mission design for asteroid 2013 PDC-E

In April 2013, the 2013 IAA Planetary Defense Conference was held in Flagstaff, AZ, USA. As a part of the conference, there was a time set aside for a dedicated Mitigation Response and Disaster Management Exercise where a fictitious asteroid named 2013 PDC-E was revealed to be on a potential impact trajectory with Earth. This 300-m asteroid was expected to have a close encounter with the Earth on November 22, 2023 where it may impact the planet or pass through a keyhole to then impact the planet later in the future. As the exercise progressed, the participants were informed that the asteroid would not impact the Earth in 2023, but instead would pass through a keyhole that would set it into a resonance orbit with the Earth that would result in an Earth impact on November 29, 2028. The purpose of the exercise was to entertain the idea of an Earth-threatening asteroid and simulate the reaction of the participants fulfilling roles ranging from characterization of the object, mitigation techniques, the

United Nations, and the general public. This section will go through hypothetical mission scenarios using pre- and post-keyhole data of the asteroid, as well as an analysis of the asteroid's encounter characteristics.

4.1. Pre-keyhole mission designs

On a trajectory to have a close-encounter with Earth, asteroid 2013 PDC-E was discovered early enough where, if we assume that we are launch capable at the time of discovery, deflection/disruption missions could be launched prior to the encounter date. In order to diminish the threat to the Earth, disruption missions will be entertained to attempt to destroy or at least deflect the asteroid from its current trajectory to avoid impacting the planet and/or the keyhole on the resulting target plane. Two mission types will be explored for this pre-keyhole trajectory: (i) short mission duration with a long dispersion time and (ii) long mission duration with a long dispersion time. Given the danger that the asteroid poses to Earth, there should exist plenty of opportunities to launch spacecraft to the body – especially closer to the encounter date. The porkchop plot for missions to the asteroid, pre-2023 encounter shown in

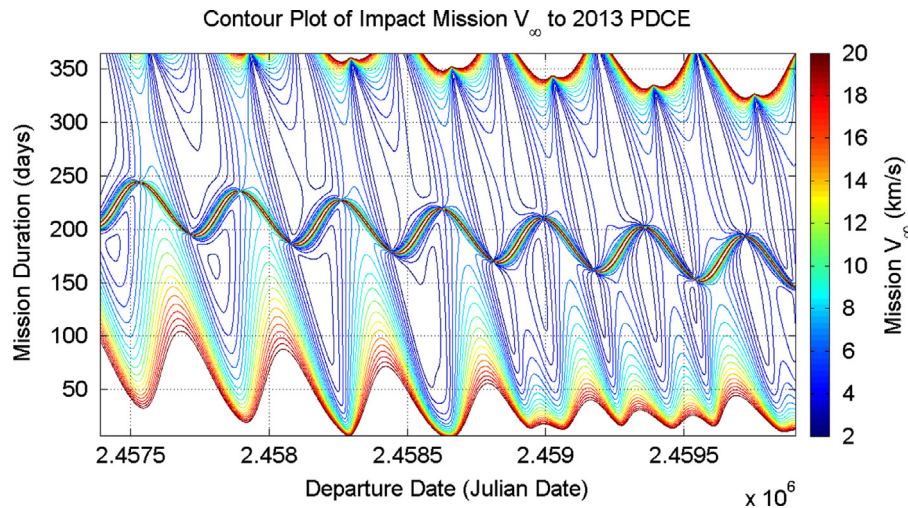


Fig. 8. Mission contour plot of total ΔV in terms of launch date and mission flight time for the pre-encounter trajectory of asteroid 2013 PDC-E.

Table 2

Optimal constrained mission parameters for a short-duration, long-dispersion pre-keyhole mission to asteroid 2013 PDC-E.

Parameter	Value
Departure date	March 7, 2019
Flight time (days)	90
Departure ΔV (km/s)	3.218
Dispersion time (days)	1631

Table 3

Mission design parameters for a short-duration, long-dispersion pre-keyhole intercept mission to asteroid 2013 PDC-E.

Mission parameter	Value
Asteroid	2013 PDC-E
LEO altitude (km)	185
Spacecraft designation	Kinetic impactor
Total HAIIV mass (kg)	2000
Departure ΔV (km/s)	3.218
C3 (km^2/s^2)	0.6396
Launch vehicle	Delta IV medium
Departure date	March 7, 2019
Mission duration (days)	90
Arrival angle (deg)	11.146
Impact velocity (km/s)	5.934
Arrival date	June 5, 2019
Estimated mission cost (\$)	904 M

Fig. 8 agree with this assessment. Missions with short dispersion times are not considered in this part of the analysis since the result is to allow for the asteroid time to miss the Earth and the keyhole on its encounter, short deflection times would not allow for effective perturbation of the asteroid.

4.1.1. Short-duration, long-dispersion, pre-keyhole mission

Launching a mission with a short mission duration and a long deflection time before encounter should result in a minimal ΔV mission that would allow plenty of time for the fragmented asteroid to avoid the important areas of the target plane (i.e. the Earth and the gravitational keyhole). For this mission type, the upper bound for the mission duration will be set for 90 days and the dispersion time will be set for anything between 200 days and 7 years. With such a wide range for the dispersion time, the best solution should tend to lean towards the upper bound. Assuming a spacecraft mass of 2000 kg, the locally optimal mission design parameters are shown in Table 2.

For these mission parameters, the preliminary mission design result is provided in Table 3.

The resulting mission has a low C3 of about $0.64 \text{ km}^2/\text{s}^2$, meaning that with a spacecraft mass of 2000 kg, most launch vehicles would be capable of injecting the spacecraft into the desired impact trajectory – in this case a Delta IV Medium would be the smallest of those launch vehicles. An impact in June 2019 leaves about four and a half years of time for the asteroid, or asteroid fragments, to be perturbed

from the original Earth-impacting trajectory. The relatively high speed at which the spacecraft would impact the asteroid and the amount of dispersion time there would be before its Earth impact seems to imply that a kinetic impactor spacecraft may be sufficient enough to perturb the asteroid from an Earth impacting or resonance orbit trajectory upon its 2023 encounter. In the case that the mission would prove unsuccessful, there would be time to launch another mission to either try and perturb the asteroid more or disrupt it before encounter.

4.1.2. Long-duration, long-dispersion, pre-keyhole mission

While the ΔV in the short-duration, long-dispersion mission is not very large that is likely due to the wide range of dispersion time allowed. However, that change in velocity can probably be brought down a little more if a longer mission duration is allowed. So, for this particular analysis the dispersion time range is kept the same (200 days to about 7 years), but the mission duration is allowed to take up to a year instead of 2 months. Looser constraints such as these should result in a cheaper mission, in terms of ΔV . Once again assuming a spacecraft

mass of 2000 kg, the optimized mission design variables for this particular scenario are presented in Table 4.

Interestingly, widening the range of mission durations results in a mission that does have a longer flight time with a lower ΔV , but the dispersion time drops considerably to a little less than a year. There are many other solutions that fit the criteria and have longer dispersion times. However, since the single over-arching criteria to determine the optimal mission design given the constrained parameters is mission ΔV , this smaller dispersion time mission is the better mission design by AMiDST.

Table 4

Optimal constrained mission parameters for a long-duration, long-dispersion pre-keyhole mission to asteroid 2013 PDC-E.

Parameter	Value
Departure date	January 5, 2022
Flight time (days)	328
Departure ΔV (km/s)	3.19
Dispersion time (days)	358

Table 5

Mission design parameters for a long-duration, long-dispersion pre-keyhole intercept mission to asteroid 2013 PDC-E.

Mission parameter	Value
Asteroid	2013 PDC-E
LEO altitude (km)	185
Spacecraft designation	HAIV
NED mass (kg)	300
Total HAIV mass (kg)	2000
Departure ΔV (km/s)	3.19
C3 (km^2/s^2)	0.0402
Launch vehicle	Delta IV medium
Departure date	January 5, 2022
Mission duration (days)	328
Arrival angle (deg)	9.77
Impact velocity (km/s)	5.126
Arrival date	November 29, 2022
Estimated mission cost (\$)	811 M

The design result for these mission parameters is provided in Table 5.

Despite the low C3 orbit that would be required to put the spacecraft into an impacting trajectory with 2013 PDC-E, the impact would be between the spacecraft and the asteroid would still be in the hypervelocity regime. This would imply that while the preferred spacecraft configuration would be a kinetic impactor due to the high speed impact, the HAIV concept would serve as a better alternative due to the shortened dispersion time before encounter [7,8]. Also, it is interesting to note that the total cost of the mission dropped a little bit despite the fact that the same launch vehicle can be used for both missions. The reason for this is that the mass of the NED is not used in the calculation of the spacecraft cost. The mission orbit is shown in Fig. 9. Given the small C3 orbit that the launch vehicle would place the spacecraft into, it makes sense that the spacecraft would essentially enter into an Earth-trailing orbit that would impact the asteroid after the Earth has passed the intersection between the asteroid's and its own orbit (Fig. 10).

While attempting to deflect/disrupt a hazardous object before its close-encounter with the Earth is a rather aggressive approach to planetary defense, the two types of mission designs presented here are a bit on the conservative end of the spectrum. The missions are relatively low risk in the sense that if the spacecraft were a kinetic impactor they would not impart very much ΔV to the asteroid and could be deemed a demonstration of our ability to intercept the body, and using a HAIV concept spacecraft could result in the same end goal or could attempt at nullifying the threat early before any real danger arose. The following mission designs for the post-encounter asteroid trajectory are much more aggressive given that the end result would be complete disruption of asteroid 2013 PDC-E.

4.2. Post-keyhole mission designs

Upon its encounter with the Earth, 2013 PDC-E passes through a keyhole on the 2023 target plane. The resulting

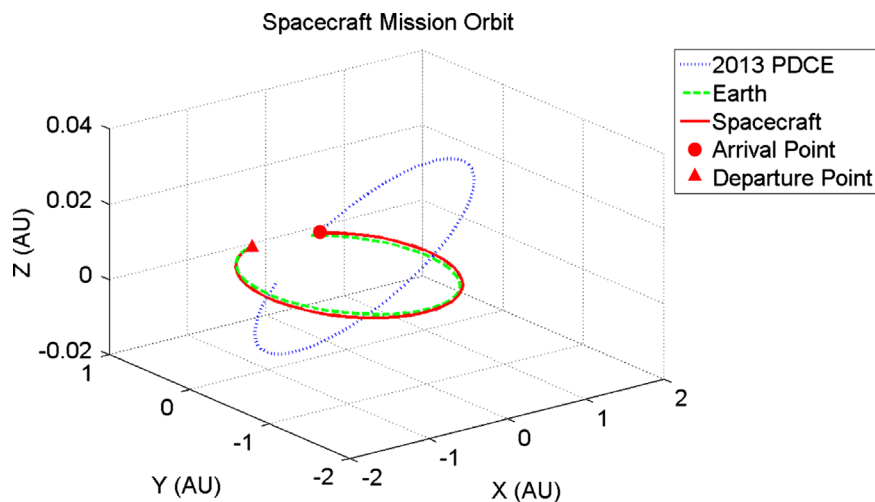


Fig. 9. Mission orbit diagram for a long-duration, long-dispersion pre-keyhole mission to asteroid 2013 PDC-E before its planetary encounter in 2023.

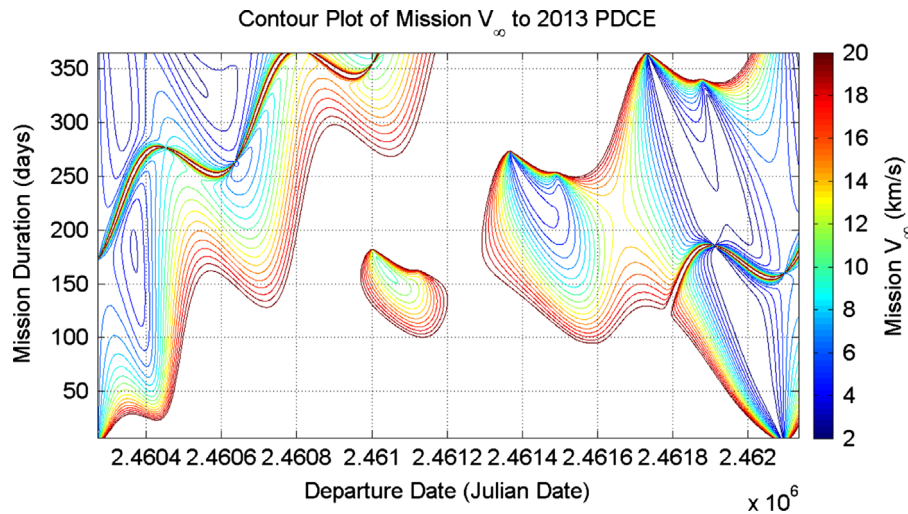


Fig. 10. Mission contour plot of total ΔV in terms of launch date and mission flight time for the post-keyhole trajectory of asteroid 2013 PDC-E.

asteroid trajectory has a 4:5 resonance with the Earth, meaning that the asteroid will impact the Earth after four of its own orbits and five of the Earth's. To deal with the certain threat to the Earth, four fictional mission types will be discussed as potential mission scenarios: (i) long-duration, long-dispersion, (ii) short-duration, long-dispersion, (iii) long-duration, short-dispersion, and (iv) short-duration, short dispersion. The purpose of these missions would be to disrupt the asteroid, given that 5 years may not be enough time to perturb the asteroid enough to avoid a collision with the Earth, in hopes to fragment the asteroid to the point that the damage on the ground would be minimal or not at all. In order to fragment the asteroid, the HAIV spacecraft will have a total mass of 3500 kg containing a 1000-kg NED.

Observing the porkchop plot for the post-keyhole trajectory of asteroid 2013 PDC-E, there is a striking difference to the contour map of the pre-keyhole trajectory. While the pre-keyhole contour shows small regions throughout the launch date domain (around 200-day mission durations) that would likely result in infeasible mission designs, the post-keyhole contour has entire regions where the required mission ΔV is high enough that it is easy to see that any mission from that region would be infeasible. On the other hand, like the pre-keyhole contour map, there are clearly evident regions where missions should be relatively easy to construct – particularly those close to the encounter date in 2023 and the anticipated impact date in 2028.

4.2.1. Long-duration, long-dispersion, post-keyhole mission

Prioritizing lower ΔV with longer dispersion times and long mission durations should result in very feasible missions for 2013 PDC-E. The only real constraint for this particular scenario is on the dispersion time, the spacecraft must impact the asteroid at least 200 days before the expected impact date. Given this relatively unconstrained situation, the optimal mission parameters for a long-term, long-dispersion mission are shown in Table 6. The mission flight time comes out to be 359 days from the launch date of July 5, 2024, resulting in an impact date of June 29, 2025

Table 6

Optimal constrained mission parameters for a long-duration, long-dispersion post-keyhole mission to asteroid 2013 PDC-E.

Parameter	Value
Departure date	July 5, 2024
Flight time (days)	359
Departure ΔV (km/s)	3.328
Dispersion time (days)	1249

Table 7

Mission design parameters for a long-duration, long-dispersion post-keyhole intercept mission to asteroid 2013 PDC-E.

Mission parameter	Value
Asteroid	2013 PDC-E
LEO altitude (km)	185
Spacecraft designation	HAIV
NED mass (kg)	1000
Total HAIV mass (kg)	3500
Departure ΔV (km/s)	3.328
C3 (km^2/s^2)	3.08
Launch vehicle	Delta IV M+(4,2)
Departure date	July 5, 2024
Mission duration (days)	359
Arrival angle (deg)	17.30
Impact velocity (km/s)	8.78
Arrival date	June 29, 2025
Estimated mission cost (\$)	1068 M

and a dispersion time of about three and a half years (Table 7).

Using the parameters from Table 6, a complete mission design with a 3500-kg HAIV spacecraft can be performed. The hyperbolic orbit that the spacecraft would be placed into has a C3 value of about $3.08 \text{ km}^2/\text{s}^2$, and a Delta IV M+(4,2) is the smallest launch vehicle with the capability to lift the spacecraft into its impacting trajectory.

Upon arriving at the asteroid, the spacecraft would have a relative impact velocity of about 9 km/s and arrival angle of a little less than 18° . A mission orbit is shown in

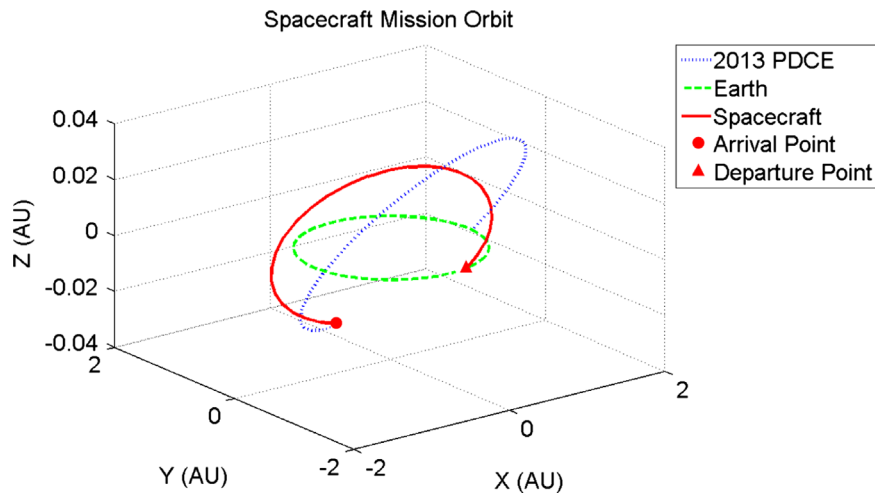


Fig. 11. Mission orbit diagram for a long-duration, long-dispersion post-keyhole mission to asteroid 2013 PDC-E after its 2023 encounter.

Fig. 11. The blue dotted trajectory is that of the asteroid, green dashed is the Earth's trajectory and the red solid trajectory shows the spacecraft's path from launch at Earth to impact with the asteroid. With such a relatively low impact velocity, the only way to protect the Earth from the asteroid threat would be the energy from the detonation of the NED used to fracture the asteroid. The estimated mission cost is just over a billion dollars, mostly due to the mass of the HAIV spacecraft.

4.2.2. Short-duration, long-dispersion, post-keyhole mission

Rating the length of dispersion time as a more important design parameter than the mission duration would result in a short-term, long-dispersion mission to asteroid 2013 PDC-E. For this scenario, the mission duration is limited to 90 days or less and the dispersion time is still bounded between 200 days and 5 years.

Interestingly enough, by minimizing the mission ΔV , given the previously mentioned constraints on the mission duration and dispersion time variables, the resulting optimal mission design would have a launch date of March 26, 2024. The spacecraft would have to be ready to launch with very little time to analyze the post-keyhole orbit. In addition to the encounter-date launch date, minimizing ΔV results in mission duration of 7 years, almost 5 years of dispersion time to the anticipated impact date. The associated departure velocity from low-Earth orbit is considerably larger than the long-duration, long-dispersion mission counterpart.

With the optimized mission parameters given in Table 8, the corresponding mission design variables are provided in Table 9. The C3 orbit required to put the spacecraft on its impact trajectory with asteroid 2013 PDC-E is very energetic and could be accomplished using an Atlas V 431 launch vehicle. With the large-C3 hyperbolic orbit the spacecraft's relative impact velocity with the asteroid is nearly 10 km/s, at an impact angle of 19.26°. The estimated mission cost is almost 1.1 billion dollars, with the difference in cost between this scenario and the long-term, long-dispersion

Table 8

Optimal constrained mission parameters for a short-duration, long-dispersion post-keyhole mission to asteroid 2013 PDC-E.

Parameter	Value
Departure date	March 26, 2024
Flight time (days)	90
Departure ΔV (km/s)	4.225
Dispersion time (days)	1619

Table 9

Mission design parameters for a short-duration, long-dispersion post-keyhole intercept mission to asteroid 2013 PDC-E.

Mission parameter	Value
Asteroid	2013 PDC-E
LEO altitude (km)	185
Spacecraft designation	HAIV
NED mass (kg)	1000
Total HAIV mass (kg)	3500
Departure ΔV (km/s)	4.225
C3 (km^2/s^2)	23.84
Launch vehicle	Atlas V 431
Departure date	March 26, 2024
Mission duration (days)	90
Arrival angle (deg)	19.26
Impact velocity (km/s)	9.89
Arrival date	June 24, 2024
Estimated mission cost (\$)	1088 M

mission coming from the larger launch vehicle being used in this mission design.

4.2.3. Long-duration, short-dispersion, post-keyhole mission

With the completion of the long-dispersion missions, the missions transition into the time frames where the impact date is not too far down the road and the missions become more and more last-minute scenarios. For this mission design,

the mission duration is allowed to go as high as a year but the dispersion time is limited between 7 and 60 days. Again, minimizing the mission ΔV within the field of potential candidate missions that fit the given criteria, the mission parameters from Table 10 are found. Leaving just 8 days for the disrupted asteroid fragments to disperse, the identified mission would have a launch date of March 4, 2028 and a mission duration of 262 days.

The overall mission architecture is described in Table 11. The mission only allows for 8 days of dispersion time with

Table 10
Optimal constrained mission parameters for a long-duration, short-dispersion post-keyhole mission to asteroid 2013 PDC-E.

Parameter	Value
Departure date	March 4, 2028
Flight time (days)	262
Departure ΔV (km/s)	3.189
Dispersion time (days)	8

Table 11
Mission design parameters for a long-duration, short-dispersion post-keyhole intercept mission to asteroid 2013 PDC-E.

Mission parameter	Value
Asteroid	2013 PDC-E
LEO altitude (km)	185
Spacecraft designation	HAIV
NED mass (kg)	1000
Total HAIV mass (kg)	3500
Departure ΔV (km/s)	3.189
C3 (km^2/s^2)	0.00019
Launch vehicle	Delta IV M+(4,2)
Departure date	March 4, 2028
Mission duration (days)	262
Arrival angle (deg)	15.21
Impact velocity (km/s)	8.435
Arrival date	November 21, 2028
Estimated mission cost (\$)	1068 M

the arrival date of the spacecraft being on November 21, 2028, with an impact angle between the spacecraft and the asteroid that is just a bit over 15° , with a relative impact speed of about eight and a half kilometers per second. This shallow, high speed impact makes sense considering the C3 orbit required for this mission is extremely small and at the time of intercept the asteroid is making its approach on Earth, Fig. 12 shows the trajectories of the Earth, asteroid, and spacecraft in dashed green, dotted blue and solid red lines, respectively (Table 12).

4.2.4. Short-duration, short-dispersion, post-keyhole mission

A short-term, short-dispersion mission is considered to be a last resort option for Earth, when time is of the essence and there are no options left. With a mission duration upper bound of 90 days and a dispersion time set to be between 7 and 90 days, AMiDST deemed this mission design the easiest to complete with at most 6 months of warning. The selected mission has a flight time that runs into the upper bound of the allowable range, given that more mission flight time generally means lower mission ΔV . With only a slightly smaller ΔV of about 3.189 km/s, this mission also results in a dispersion time of 8 days after a 89-day cruise to the asteroid following an August 24, 2028 launch date.

The mission design parameters for this short-duration, short-dispersion mission, shown in Table 13, are not very different from those of the long-duration, short-dispersion mission discussed previously. An arrival angle of about 17.8°

Table 12
Optimal constrained mission parameters for a short-duration, short-dispersion post-keyhole mission to asteroid 2013 PDC-E.

Parameter	Value
Departure date	August 24, 2028
Flight time (days)	89
Departure ΔV (km/s)	3.189
Dispersion time (days)	8

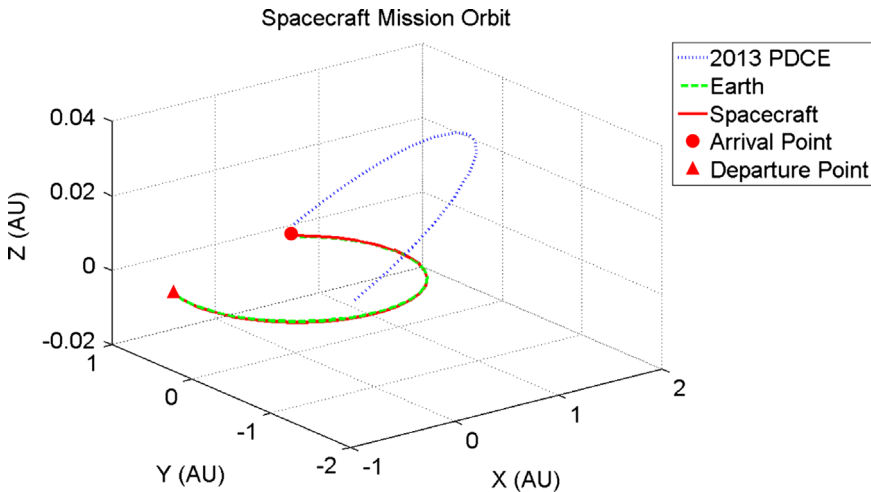


Fig. 12. Mission orbit diagram for a long-duration, short-dispersion mission to asteroid 2013 PDC-E after its 2023 encounter.

Table 13

Mission design parameters for a short-duration, short-dispersion post-keyhole intercept mission to asteroid 2013 PDC-E.

Mission parameter	Value
Asteroid	2013 PDC-E
LEO altitude (km)	185
Spacecraft designation	HAIV
NED mass (kg)	1000
Total HAIV mass (kg)	3500
Departure ΔV (km/s)	3.189
C3 (km ² /s ²)	0.0008
Launch vehicle	Delta IV M+(4,2)
Departure date	August 24, 2028
Mission duration (days)	89
Arrival angle (deg)	17.834
Impact velocity (km/s)	9.81
Arrival date	November 21, 2028
Estimated mission cost (\$)	1068 M

this time is only slightly larger than the previous 15.2°, and the relative impact speed increased a bit to over 9.8 km/s. Also, not surprisingly, the estimated mission costs for three of these four post-keyhole mission designs (long-duration/long-dispersion, long-duration/short-dispersion, short-duration/short-dispersion) have all been the same – given the size of the spacecraft has not changed and the desired launch vehicle is a Delta IV M+(4,2).

4.3. Post-keyhole mission design summary

Each of the six missions analyzed in this section for hypothetical post-keyhole missions, with its own time and place, are completely feasible and would probably result in the asteroid, or a majority of the asteroid's fragmented mass, not impacting the Earth. Making an attempt on the threatening body as early as possible would give some time afterwards in case something were to go wrong and/or the mission were to fail. But, this post-keyhole mission design assumed that we are ready to launch a spacecraft upon discovering a threat, if not, then this scenario is meaningless. If the basic assumption of launch readiness is taken as truth, then the best course of action for the asteroid 2013 PDC-E would have been to impact the asteroid long before its 2023 keyhole encounter with Earth – employing one of the first two mission designs. If there is hesitation towards that idea based on the potential of perturbing the asteroid into an Earth-impacting trajectory or a resonant trajectory, then what may be considered a more suitable course of action would be to allow the asteroid to have its encounter with the Earth and plan a mission based on its altered trajectory.

Planning a mission based on the altered orbit trajectory of 2013 PDC-E would mean that the first two of the post-keyhole mission designs would be under consideration. However, the short-duration, long-dispersion mission launching on the encounter date may be a little of an optimistic plan. There may not be enough time to analyze asteroid's new orbital trajectory to see if a disruption mission is even deemed necessary. If it is absolutely necessary and the time has grown short, the last option for mankind should be to launch a mission with a short-dispersion time (either of the last two

mission designs). But, it cannot be stressed enough that option should not be taken as the only plan of attack in hopes that new information would make the asteroid less of a threat – early action is best. Regardless, any action may be better than inaction.

5. Conclusions

This paper has presented the on-going research work at Asteroid Deflection Research Center on further developing a high-fidelity gravitational simulator and characterizing post-encounter orbital variations as applied to planetary defense mission trajectory design. As an example of Earth-impacting asteroids passing through keyholes, a fictitious asteroid 2013 PDC-E was used to demonstrate the effectiveness of using AMiDST for various pre-keyhole as well as post-keyhole mission designs.

Acknowledgments

This research has been supported in part by NASA's Iowa Space Grant Consortium and a NIAC Phase 2 study (2012–2014). The authors would like to thank William Harding, undergraduate student at Iowa State University, for his technical assistance with some of the improvements to AMiDST. Also, the authors would like to give special thanks to Dr. Paul Chodas for the information and advice he has provided to us on both analytic and numerical keyhole computations.

Appendix A. An overview of keyhole theory

A.1. Target planes

A target plane is defined as a geocentric plane oriented to be normal to the asteroid's geocentric velocity vector. By observing the point of intersection of an asteroid trajectory with the target plane can lend significant insight into the nature of a future encounter. In general, there are two distinct planes and several coordinate systems that can be used in such a framework. The classical target plane is referred to as the B-plane, which has been used in astrodynamics since the 1960s. The B-plane is oriented normal to the incoming asymptote of the geocentric hyperbola, or normal to the unperturbed relative velocity \mathbf{v}_∞ . The plane's name is a reference to the so-called impact parameter b , the distance from the geocenter to the intercept of the asymptote on this plane, known as the minimum encounter distance along the unperturbed trajectory [16]. Fig. 13 depicts the relationship between the target B-plane and the trajectory plane of the asteroid. The system of coordinates that will be used for the analyses conducted in this paper are described later, those shown on the figure are just an example that could be used.

A.2. Target plane coordinates

Generally it is convention to place the origin of the B-plane's coordinate system at the geocenter, but the orientation of the coordinate axes on the plane is arbitrary.

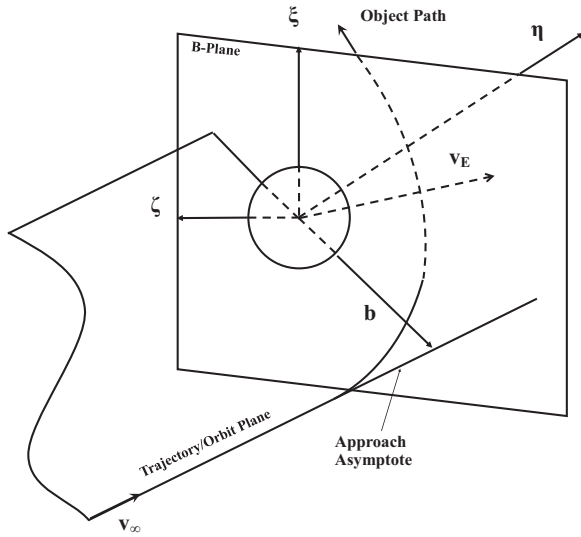


Fig. 13. Representation of the target B-plane of a planet with respect to the incoming approach of a body on the trajectory plane.

The system has been fixed at times by aligning the axes in a way so that one of the nominal target plane coordinates is zero, or by aligning one of the coordinate axes with either the projection of the Earth's polar axis or the projection of the Earth's heliocentric velocity.

One of the most important functions of the target plane is to determine whether a collision is possible, and if not, how deep the encounter will be. With the B-plane, we obtain the minimum distance of the unperturbed asteroid orbit at its closest approach point with the Earth – the impact parameter b . That single variable however does not tell whether the asteroid's perturbed trajectory will intersect the image of the Earth on the following encounter, but the information can be extracted by scaling the Earth radius R_{\oplus} according to the following relationship

$$b_{\oplus} = R_{\oplus} \sqrt{1 + \frac{v_e^2}{v_{\infty}^2}} \quad (\text{A.1})$$

where v_e is the Earth escape velocity

$$v_e = \sqrt{\frac{2GM_{\oplus}}{R_{\oplus}}} \quad (\text{A.2})$$

With this formulation a given trajectory impacts the Earth if $b < b_{\oplus}$, and would not otherwise. Alternatively, the impact parameter could be scaled while leaving the image of the Earth on the B-plane unchanged. The two scalings are equivalent for a single orbit, but when computing the coordinates for different asteroids with different v_{∞} , the scaling is not uniform [17].

A convenient and common target plane coordinate system (ξ, η, ζ) is obtained by aligning the negative ζ -axis with the projection of the Earth's heliocentric velocity \mathbf{V}_{\oplus} , the positive η -axis with the geocentric velocity of the incoming body (normal to the B-plane), and the positive ξ -axis in such a way that the reference frame is positively

oriented, expressed by the following:

$$\eta = \frac{\mathbf{U}}{\|\mathbf{U}\|} \quad (\text{A.3})$$

$$\xi = \frac{\eta \times \mathbf{V}_{\oplus}}{\|\eta \times \mathbf{V}_{\oplus}\|} \quad (\text{A.4})$$

$$\zeta = \xi \times \eta \quad (\text{A.5})$$

where U and U are the geocentric velocity textbftor and magnitude of the asteroid, respectively. With this reference frame, it can be seen that ξ and ζ are on the B-plane itself, where (ξ, ζ) are the target plane coordinates that indicate the cross track and along track miss distances, respectively. That way, ζ is the distance in which the asteroid is early or late for the minimum possible encounter distance. The ξ coordinate, on the B-plane, refers to the minimum distance achieved by altering the timing of the encounter between the asteroid and the Earth, known as the Minimum Orbital Intersection Distance (MOID). It is important to note that this particular interpretation of the coordinates of the B-plane is only valid in the linear approximation, and unusable for distant encounters beyond several lunar distances.

Such a formulation of the problem gives rise to the thought that an asteroid can avoid impact if either the timing of the encounter is off or by being in an orbit that does not even intersect the Earth's orbit. Therefore, to have an impact occur the asteroid must have a small enough MOID and be on time for the encounter. So, an encounter can be well-defined given only the MOID and the time of the encounter. The manner in which the encounters are characterized in this paper are according to the analytic theory developed by Valsecchi et al. [17].

A.3. Resonant returns and keyholes

A resonant return orbit is a consequence of an encounter with Earth, such that the asteroid is perturbed into an orbit of period $P' \approx k/h$ years, with h and k integers. After h revolutions of the asteroid and k revolutions of the Earth, both bodies are in the same region of the first encounter, causing a second encounter between the asteroid and the Earth.

The analytic theory of resonant returns that has been developed by Valsecchi et al. [17] treats close encounters with an extension of Opik's theory, adding a Keplerian heliocentric propagation between the encounters. The heliocentric propagation establishes a link between the outcome of the first encounter and the initial conditions of the next one. During the Earth encounter, the motion of the asteroid is assumed to take place on one of the asymptotes of the encounter hyperbola. The asymptote is directed along the unperturbed geocentric encounter velocity \mathbf{v}_{∞} , crosses the B-plane at a right angle, and the vector from the Earth to the intersection point is denoted by \mathbf{B} [16].

According to Opik's theory, the encounter of the asteroid with the Earth consists of the instantaneous transition, when the body reaches the B-plane, from the pre-encounter velocity textbftor \mathbf{v}_{∞} to the post-encounter velocity textbftor \mathbf{v}'_{∞} , such that $v'_{\infty} = v_{\infty}$. And, the angles θ' and ϕ' are simple functions of v_{∞} , θ , ϕ , ξ , and ζ , where θ is the angle between \mathbf{v}_{∞} and the

Earth's heliocentric velocity \mathbf{V}_{\oplus} and ϕ is the angle between the plane containing \mathbf{v}_{∞} and \mathbf{V}_{\oplus} and the plane containing \mathbf{V}_{\oplus} and the ecliptic pole. The deflection angle γ is the angle between \mathbf{v}_{∞} and \mathbf{v}'_{∞} , described by

$$\tan \frac{\gamma}{2} = \frac{c}{b} \quad (\text{A.6})$$

where $c = GM_{\oplus}/v_{\infty}^2$. In addition, simple expressions relate (a, e, i) to $(v_{\infty}, \theta, \phi)$, and (ω, Ω, ν) to (ξ, ζ, t_0) , where t_0 is the time at which the asteroid passes the node closer to the encounter [16,17].

A resonance orbit corresponds to certain values of a' and θ' , that can be denoted by a'_0 and θ'_0 . If the post-encounter is constrained in such a way that the ratio of periods between the Earth and the asteroid is k/h , then we have

$$a'_0 = \left(\frac{k}{h}\right)^{2/3} \quad (\text{A.7})$$

$$\cos \theta'_0 = \frac{1 - U^2 - 1/a'_0}{2U}$$

$$\cos \theta'_0 = \cos \theta \frac{b^2 - c^2}{b^2 + c^2} + \sin \theta \frac{2c\zeta}{b^2 + c^2} \quad (\text{A.8})$$

Thus, for a given U , θ , and θ'_0 , we have

$$\cos \theta'_0 = \cos \theta \cos \gamma + \sin \theta \sin \gamma \cos \psi \quad (\text{A.9})$$

in the pre-keyhole B-plane, which gives the locus of points leading to a given resonant return.

References

- [1] General Mission Analysis Tool (GMAT), National Aeronautics and Space Administration Goddard Space Flight Center. (<http://gmatt.gsfc.nasa.gov/index.html>), May 2012.
- [2] LTTT Suite Optimization Tools, in: A. Timothy Reckart (Ed.), NASA Glenn Research Center Space Science Projects Office, 23 April 2012. (<http://microgravity.grc.nasa.gov/SSPO/ISPTProg/LTTT/>), May 2012.
- [3] N. Melamed, Development of a handbook and an on-line tool on defending Earth against potentially hazardous objects, *Acta Astronaut.* 90 (1) (2013) 165–172. (<http://dx.doi.org/10.1016/j.actaastro.2012.03.021>).
- [4] G. Vardaxis, B. Wie, Asteroid mission design software tool for planetary defense applications, in: AIAA 12–4872, AIAA/AAS Astrodynamics Specialist Conference, August 2012.
- [5] G. Vardaxis, A. Pitz, B. Wie, Conceptual design of planetary defense technology demonstration mission, in: AAS 12–128, AAS/AIAA Space Flight Mechanics Meeting, February 2012.
- [6] G. Vardaxis, B. Wie, Development of an asteroid mission design software tool for planetary defense, in: IAA-PDC13–04–07, 2013 Planetary Defense Conference, Flagstaff, AZ, April 15–19, 2013.
- [7] A. Pitz, B. Kaplinger, B. Wie, Preliminary design of hypervelocity nuclear interceptor spacecraft for disruption/fragmentation of NEOs, in: AAS 12 225, AAS/AIAA Space Flight Mechanics Meeting, Charleston, SC, January 30–February 2, 2012.
- [8] A. Pitz, B. Kaplinger, G. Vardaxis, T. Winkler, B. Wie, Conceptual design of a hypervelocity asteroid intercept vehicle and its flight validation mission, *Acta Astronaut.* 94 (2014) 42–56.
- [9] Near-Earth Object Program, Near-Earth Object Program, in: Donald K. Yeomans (Ed.), National Aeronautics and Space Administration, (<http://neo.jpl.nasa.gov/index.html>), May 2013.
- [10] P.W. Chodas, D. Yeomans, Orbit determination and estimation of impact probability for near Earth objects, in: AAS 09–002, AAS/AIAA Space Flight Mechanics Meeting, 2009.
- [11] A. Pitz, C. Teubert, B. Wie, Earth-impact probability computation of disrupted asteroid fragments using GMAT/STK/CODES, in: AAS 11–408, AAS/AIAA Astrodynamics Specialist Conference, August 2011.
- [12] D.K. Yeomans, P.W. Chodas, G. Sitarski, S. Szutowicz, M. Krolukowska, Cometary Orbit Determination and Nongravitational Forces, Comets II, The Lunar and Planetary Institute, 2004, pp. 137–152.
- [13] Near-Earth Object Survey and Deflection Study Report, NASA, 2006.
- [14] Defending Planet Earth: Near-Earth Object Surveys and Hazard Mitigation Strategies, Report No. 0-309-14968-1, National Research Council, National Academy of Sciences, 2010.
- [15] A. Carusi, G.B. Valsecchi, R. Greenberg, Planetary close encounters: geometry of approach and post-encounter orbital parameters, *Celest. Mech. Dyn. Astron.* 49 (1990) 111–131.
- [16] A. Milani, S.R. Chesley, P.W. Chodas, G.B. Valsecchi, Asteroid Close Approaches: Analysis and Potential Impact Detection, Asteroids III, The Lunar and Planetary Institute, 2002, p. 55–69.
- [17] G.B. Valsecchi, A. Milani, P.W. Chodas, S.R. Chesley, Resonant returns to close approaches: analytic theory, *Astron. Astrophys.* 408 (2003) 1179–1196.